

# Foundation Models for ECG: Leveraging Hybrid Self-Supervised Learning for Advanced Cardiac Diagnostics

Junho Song  
jhsong@medicalai.com  
AI Group, Medical AI Co., Ltd.  
Seoul, Republic of Korea

Jong-Hwan Jang  
jangood1122@medicalai.com  
AI Group, Medical AI Co., Ltd.  
Seoul, Republic of Korea

Byeong Tak Lee  
bytaklee@medicalai.com  
AI Group, Medical AI Co., Ltd.  
Seoul, Republic of Korea

DongGyun Hong  
dghong@medicalai.com  
AI Group, Medical AI Co., Ltd.  
Seoul, Republic of Korea

Joon-myung Kwon  
cto@medicalai.com  
AI Group, Medical AI Co., Ltd.  
Seoul, Republic of Korea

Yong-Yeon Jo  
yy.jo@medicalai.com  
AI Group, Medical AI Co., Ltd.  
Seoul, Republic of Korea

## Abstract

Using foundation models enhanced by self-supervised learning (SSL) methods presents an innovative approach to electrocardiogram (ECG) analysis, which is crucial for cardiac health monitoring and diagnosis. This study comprehensively evaluates foundation models for ECGs, leveraging SSL methods, including generative and contrastive learning, on a vast dataset comprising approximately 1.3 million ECG samples. By integrating these methods with consideration of the unique characteristics of ECGs, we developed a Hybrid Learning (HL) for foundation models that improve the precision and reliability of cardiac diagnostics. The HL-based foundation model adeptly captures the intricate details of ECGs, enhancing diagnostic capability. The results underscore the considerable potential of SSL-enhanced foundation models in clinical settings, setting the stage for future research into their scalable applications across a broader range of medical diagnostics. This work sets a new standard in the ECG field, emphasizing the transformative influence of tailored, data-driven model training on the effectiveness and accuracy of medical diagnostics.

## CCS Concepts

• **Applied computing** → **Health care information systems.**

## Keywords

Foundation model, Self-supervised learning, Generative learning, Contrastive learning, Electrocardiogram, Biosignal process

## ACM Reference Format:

Junho Song, Jong-Hwan Jang, Byeong Tak Lee, DongGyun Hong, Joon-myung Kwon, and Yong-Yeon Jo. 2018. Foundation Models for ECG: Leveraging Hybrid Self-Supervised Learning for Advanced Cardiac Diagnostics. In *Proceedings of ACM SIGKDD Conference on Knowledge Discovery and Data Mining (ACM KDD 2025)*. ACM, New York, NY, USA, 15 pages. <https://doi.org/XXXXXXX.XXXXXXX>

Permission to make digital or hard copies of all or part of this work for personal or classroom use is granted without fee provided that copies are not made or distributed for profit or commercial advantage and that copies bear this notice and the full citation on the first page. Copyrights for components of this work owned by others than the author(s) must be honored. Abstracting with credit is permitted. To copy otherwise, or republish, to post on servers or to redistribute to lists, requires prior specific permission and/or a fee. Request permissions from [permissions@acm.org](mailto:permissions@acm.org).

ACM KDD 2025, August 03–07, 2025, Toronto, CA

© 2018 Copyright held by the owner/author(s). Publication rights licensed to ACM.

ACM ISBN 978-1-4503-XXXX-X/18/06

<https://doi.org/XXXXXXX.XXXXXXX>

## 1 Introduction

Electrocardiograms (ECGs) are critical bio-signals that record the heart's electrical activity, offering vital information about heart rhythm, strength, timing, and beat rate. These signals are essential for diagnosing heart diseases and identifying abnormalities such as myocardial infarction, arrhythmias, and other cardiac disorders. Effective modeling of ECGs is crucial for accurate diagnosis and treatment, making advancements in this field highly impactful.

In recent years, Deep Neural Networks (DNNs) have shown great potential in analyzing ECGs and performing tasks like prediction, classification, and denoising. However, the application of DNNs faces two significant challenges. First, the sensitive nature of ECGs necessitates stringent privacy protections, leading to limited availability of labeled data. Second, the low prevalence of certain heart diseases results in insufficient labeled datasets to effectively train DNNs [17].

To address these challenges, researchers have turned to foundation models enhanced by Self-Supervised Learning (SSL) methods. These models have demonstrated significant promise across various domains, including natural language processing [2, 10], computer vision [7, 15], and speech recognition [5]. Foundation models for ECGs can leverage unlabeled data to learn robust representations, which can then be fine-tuned with minimal labeled data, making them both flexible and efficient. Utilizing the foundation model offers several key benefits:

- **Reduced Need for Labeled Data:** SSL enables training with only unlabeled data, reducing the dependency on extensive labeled datasets.
- **Enhanced Accuracy and Efficiency:** These models are able to be fine-tuned for specific tasks, achieving higher accuracy and faster convergence than models trained from scratch.
- **Cost-efficient Extensibility:** Foundation models require less cost to expand to various downstream tasks by fine-tuning, thus enhancing efficiency.

The effectiveness of foundation models hinges on robust pre-training, heavily relying on SSL methods. Two primary SSL methods are Contrastive Learning (CL) and Generative Learning (GL). CL focuses on distinguishing between similar and dissimilar instances, while GL aims to reconstruct data by predicting masked parts of the input, thereby improving the model's understanding of the data [9, 21, 25, 37].

Despite their potential, the application of foundation models for ECGs is still in its infancy. Comprehensive research is needed into various aspects, such as architectural designs, SSL methods, and practical applications. The research focuses on three main areas:

- **Architectural Designs:** Analyzing architectural designs, particularly the Vision Transformer (ViT) [11], for generalizing representations of the ECGs by balancing the local and global features.
- **SSL Methods:** Evaluating contrastive, generative, and hybrid SSL methods to determine the most effective strategy for ECG representation.
- **Practical Applicability:** Validating the models in real-world scenarios characterized by low incidence rates and limited data availability.

Through this research, we aim to fill the gaps in implementing the foundation model for ECGs. We provide empirical guidance on pre-training foundation models across various architectural designs and SSL methods and evaluate their efficacy. Furthermore, our work combines the strengths of SSL methods, called Hybrid Learning (HL), to better suit clinical needs and advance their readiness for broader healthcare applications, ultimately facilitating significant technological advancements in medical practice. Our contributions include:

- **Large-Scale ECG Dataset:** Training foundation models with large-scale ECG dataset (i.e., including about 1.3M ECGs).
- **HL-based Foundation Model:** Introducing a foundation model by a hybrid learning approach that combines SSL methods tailored for ECGs.
- **Guidance for Foundation Models:** Providing detailed insights into the performance of ECG foundation models according to their various SSL methods, architectural design, and practical applicability.

The results of this study are expected to advance the utilization of SSL-based foundational models for ECGs notably. These findings offer valuable insights into establishing a foundation model for ECGs, not only for future research but also for practical applications in clinical environments.

## 2 Related Work

### 2.1 Self-Supervised Learning Methods

SSL methods have significantly advanced the field of machine learning by allowing models to learn from vast amounts of unlabeled data. These methods have shown great promise in various domains, including the bio-signal domain, where they help develop robust data representations that can be fine-tuned for specific tasks with minimal labeled data [1, 8, 13, 19, 27, 28, 31, 32, 35, 40–42].

- **Contrastive Learning (CL):** CL focuses on improving a model's ability to form meaningful embeddings by contrasting similar and dissimilar instances. This method involves creating pairs of similar and dissimilar data points and using a contrastive loss function, such as InfoNCE, to bring similar instances closer in the embedding space while pushing dissimilar instances apart [6, 7, 16]. CL has been successfully applied in areas such as visual representation learning and natural language processing, where it enhances the model's ability to capture the underlying structure of the data and improves performance on downstream tasks.

- **Generative Learning (GL):** GL methods, such as Masked Autoencoders (MAE) [11, 15, 39], challenge models to reconstruct missing parts of the input data. This process helps the model comprehensively understand the data's structure and semantics [4]. GL methods are particularly effective in tasks like denoising and anomaly detection, as they enable the model to infer and regenerate the obscured data segments [43], thereby enhancing its predictive capabilities [26].
- **Hybrid Learning (HL):** HL combines the strengths of both CL and GL, leveraging the discriminative power of CL and the high-fidelity representation capability of GL. This synergistic method has shown promising results in various domains, such as computer vision [18], and holds significant potential for the bio-signal domain, including ECGs. By balancing these two methods, HL aims to create robust and flexible data representations that are both accurate and generalizable.

### 2.2 Applications of SSL for ECGs

SSL methods have been increasingly adopted in bio-signal applications, particularly ECGs. These methods have demonstrated substantial improvements in model accuracy and generalizability, making them invaluable for clinical diagnostics [1, 3, 23–25].

- **Innovate ECG Foundation Model:** Recent studies have shown that SSL methods significantly enhance the accuracy of ECG classification. For instance, the SSL-based models have outperformed traditional supervised learning methods [14, 31]. However, it is a very early stage; advanced architectural networks and SSL methods have been proposed and have shown successful results [15, 18, 43] in the leading domains such as NLP and vision. These advanced architectural networks and SSL methods leverage the ability to learn from vast amounts of unlabeled data, improving the ability to detect subtle patterns in ECGs.
- **Addressing Data Challenges:** One of the significant challenges in the ECG domain is the scarcity and imbalance of labeled data [17], which hinders the development of accurate diagnostic models. Self-supervised learning (SSL) methods have effectively overcome these issues by utilizing large datasets of unlabeled ECG recordings for pre-training, allowing the models to learn useful representations from abundant unlabeled data. This pre-training step helps create robust models that perform well even when labeled data is limited, ensuring reliable and accurate diagnostics in clinical settings. Moreover, SSL enhances the model's ability to generalize across different patient populations and varying clinical conditions, further increasing its practical utility in real-world applications [22].

## 3 Study Design

Our study unfolds through a meticulously structured sequence of steps, aiming to comprehensively evaluate foundation models for ECGs. The process includes data preparation, model training, thorough evaluation, and analysis steps. Figure 1 illustrates the entire procedure of our study.

### 3.1 Data Preparation

We prepare two types of datasets: unlabeled and labeled. The unlabeled dataset is compiled from five public repositories: MIMIC [20],

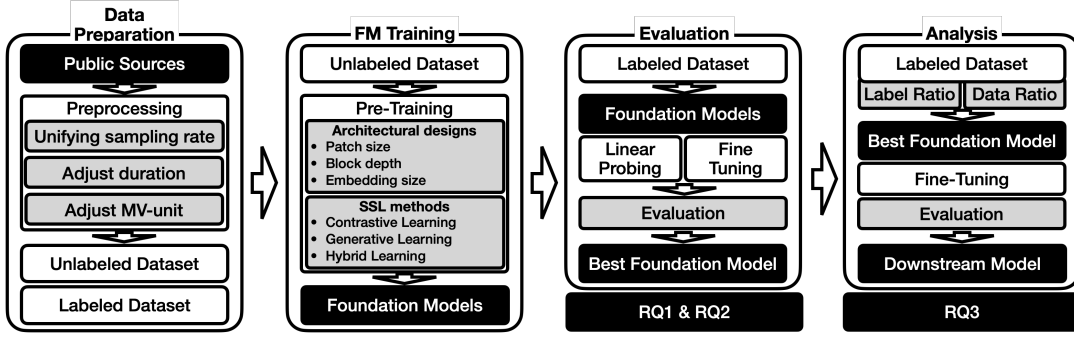


Figure 1: Study procedure.

CODE15 [29], BIOBANK [34], SAMI [30], and IKEM [33]. We select these datasets to ensure demographic fairness by including data collected from various continents. This dataset encompasses 1,291,868 ECG samples from 442,736 distinct patients, mitigating potential biases and enhancing the generalizability of the study results. See Table 6 in Appendix A for more details.

The labeled datasets utilized for the classification tasks are derived from ECGs in the PTB-XL dataset [36]. This dataset includes super-classes: Myocardial Infarction (MI), ST/T change (STTC), Conduction Disturbance (CD), and Hypertrophy (HYP), chosen to encompass the diverse morphological features and rhythmic patterns inherent in ECGs. A total of 21,265 ECG samples collected from 8,000 patients are included in this dataset, with the number of labels in each class being 1,738 for MI (25% of case ratio), 1,389 for STTC (24%), 1,269 for CD (22%), and 341 for HYP (12%). It's important to note that this labeled dataset is notably small and class-imbalanced, a well-known characteristic of medical data [17]. More details can be found in Table 7 in the Appendix A.

Before analysis, all data undergo a standardization process to account for inherent variances in sample rate, measuring duration, and measurement unit (i.e., millivolts unit that is different according to ECG recording tool, abbreviated as MV-Unit) among different datasets. To standardize our comparisons and maintain consistency across analyses, we adjust the sample rate to 250 Hz, the measurement duration to 10 seconds, and the MV-Units to 1.0, rendering each ECG signal in our dataset to consist of a 2500 length per lead.

### 3.2 Model Development

**Foundation Models.** In our study, we adopt a HL method to pre-train our foundation models, effectively integrating the strengths of both GL and CL. These models incorporate the Vision Transformer (ViT) [11] as the primary architectural backbone, modified with a one-dimensional convolution projection layer specifically tailored for embedding ECGs [38]. This comprehensive architecture allows for robust and versatile learning, making the foundation models particularly effective for ECG applications.

The overall structure of our foundation models, as depicted in Figure 2, consists of a preprocessor, an encoder, and a decoder. In Figure 2, red and blue dotted lines indicate the variations for GL and CL, respectively, on each forward propagation path. The forward propagation process is as follows:

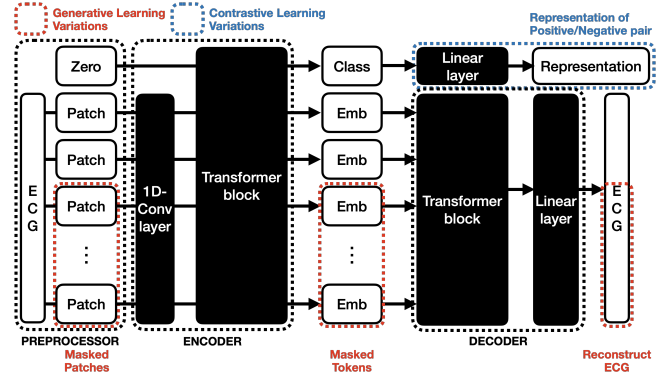


Figure 2: Structure of foundation models.

- **GL Path:** The preprocessor first masks specific patches of the ECG signal. The encoder then processes these unmasked patches and generates embeddings. The decoder uses these embeddings to reconstruct the original ECG signal. This process helps the model learn to predict missing information and understand complex data patterns.
- **CL Path:** The preprocessor creates augmented views of the ECG patches. The encoder processes these augmented patches to generate embeddings. The contrastive loss is calculated by bringing the embeddings of positive pairs closer and pushing those of negative pairs apart. This process helps the model distinguish between similar and dissimilar ECGs.

The backward propagation process is as follows:

- **Generative Loss:** The reconstruction loss, quantified using the mean absolute error (MAE), measures the difference between the original and reconstructed ECGs, which is calculated as follows:

$$L_{\text{RECON}} = \sum_{i=1}^N |x_i - y_i| \quad (1)$$

where  $x_i$  is the original signal and  $y_i$  is the reconstructed signal.

- **Contrastive Loss:** The contrastive loss measures how well the model can distinguish between similar and dissimilar pairs of ECG signal embeddings, which is calculated using the InfoNCE

loss function[7] as follows:

$$L_{\text{CONT}} = -\log \frac{\exp(z_i \cdot z_j / \tau)}{\sum_{k=0}^N \exp(z_i \cdot z_k / \tau)} \quad (2)$$

where  $(z_i)$  and  $(z_j)$  are the embeddings of the positive pair,  $(\tau)$  is a temperature parameter, and  $(N)$  is the number of negative samples.

- **Hybrid Loss:** The total hybrid loss combines the reconstruction loss and the contrastive loss to leverage the strengths of both learning strategies. It is given by:

$$L_{\text{HYBRID}} = L_{\text{RECON}} + L_{\text{CONT\_Patient}} + L_{\text{CONT\_Sample}} \quad (3)$$

where  $L_{\text{CONT\_Patient}}$  patient and  $L_{\text{CONT\_Sample}}$  are the contrastive losses calculated at the patient and sample levels, respectively. The hybrid loss enables the model to leverage both GL and CL methods together, thereby improving its capacity to comprehend and depict intricate ECG patterns. This well-rounded learning objective guarantees that the model can accurately reconstruct detailed signal information and effectively discern between various types of ECGs.

**Downstream Tasks.** After pre-training the foundation models using SSL, we employ two downstream learning strategies: linear probing and fine-tuning.

- **Linear Probing:** In linear probing, the weights in the encoder of the foundation model are frozen, and a linear classifier is added to its output layer. The linear classifier is trained using the labeled ECG dataset to evaluate the quality of the learned representations without updating the weights in the encoder of the foundation model. This approach offers insights into the utility of the pre-trained features for classification.
- **Fine-Tuning:** Tuning the whole weights in the given model, including the weights in the encoder of the foundation model and the added linear classifier, allows the model to better adapt to specific classification tasks using labeled data. This approach typically yields better performance than linear probing, as it adjusts the pre-trained features to fit the particular characteristics of the labeled dataset.

### 3.3 Evaluation and Analysis

We assess the performance of downstream models based on CL-, GL-, and HL-based foundation models and analyze the results to address the following research questions. For simplicity, we refer to the SSL-based foundation model as the SSL foundation model (i.e., CL, GL, and HL foundation model), the linear probed model on the SSL-based foundation model as the SSL linear probing model (i.e., CL, GL, and HL linear probing model), and the fine-tuned model on the SSL-based foundation model as the SSL fine-tuned model (i.e., CL, GL, and HL fine-tuned model).

#### ***RQ1. What architectural designs of foundation models are most effective for capturing the representation of ECG?***

The architectural design of the foundation model is critical in effectively generalizing representations of ECGs by balancing the local and global features of ECGs [26]. We conduct an extensive grid search to examine the impact of key parameters on the architectural design for data representation: patch size, block depth, and embedding size. The variations of each parameter are {60, 125, 250},

{2, 4, 8}, and {256, 512, 1024} respectively. Consequently, we evaluated 27 distinct foundation models in each SSL method, totaling 81 models, using linear probing. The linear probing evaluation aims to assess the generalizability of the representations of ECGs from each SSL foundation model by their performance on various downstream tasks. This methodical exploration aims to identify the architectural designs that most accurately capture the complex representations of ECGs in each SSL method.

#### ***RQ2. Which are the most adept at accurately encoding the complex representations of ECGs among the SSL methods?***

After identifying the optimal architectural design for each SSL foundation model from RQ1, we aim to compare the performance of CL, GL, and HL foundation models using linear probing with the labeled dataset across various downstream tasks. This evaluation allows us to investigate how effectively each SSL method learns generalized ECG representations that span a variety of downstream tasks. Additionally, we will provide a detailed analysis of the effectiveness of each SSL method using four distinct metrics as outlined in the risk decomposition method [12]. The risk decomposition method assists in identifying the primary sources of error and understanding the trade-offs between different SSL methods. By dissecting these error components, researchers and practitioners can effectively optimize SSL foundation models, ensuring robust and reliable performance even under challenging conditions such as class imbalance and limited resources.

#### ***RQ3. How can foundation models be effectively implemented within clinical environments to optimize diagnostic processes?***

With the labeled dataset, the first step involves assessing the performance of each SSL fine-tuned model for downstream tasks. This evaluation aims to determine how effectively each SSL foundation model can adapt to and enhance its performance on specific tasks through fine-tuning. Next, we consider real-world scenarios such as low incidence rates and limited availability of cardiac disease data [17]. We then examine the practical effectiveness of these models in addressing cardiac downstream tasks under these conditions. This investigation includes validating the robustness of each SSL fine-tuned model, ensuring that they maintain performance even under class imbalance and limited resources. To achieve this, we assess performance using labeled datasets with different case ratios and data usage settings: {5%, 2%, 1%} and {50%, 25%, 10%}. The case ratios are aligned with the real-world incidence rate [17], and the data usage settings are determined based on the available number of labels in the labeled dataset.

## 4 Experimental Results

This section presents the summary of the experimental results for the research questions. As the evaluation metrics, we used the Area Under the Receiver Operating Characteristic Curve (AUROC) and the Area Under the Precision-Recall Curve (AUPRC) for four downstream tasks: MI, STTC, CD, and HYP. Criteria denote the sum of all AUROCs and AUPROCs for each model. Due to space limitations, each subsection presents the summary of the results. See Appendix C for the complete results, and Appendix B for details of metrics.

#### 4.1 Architectural Design

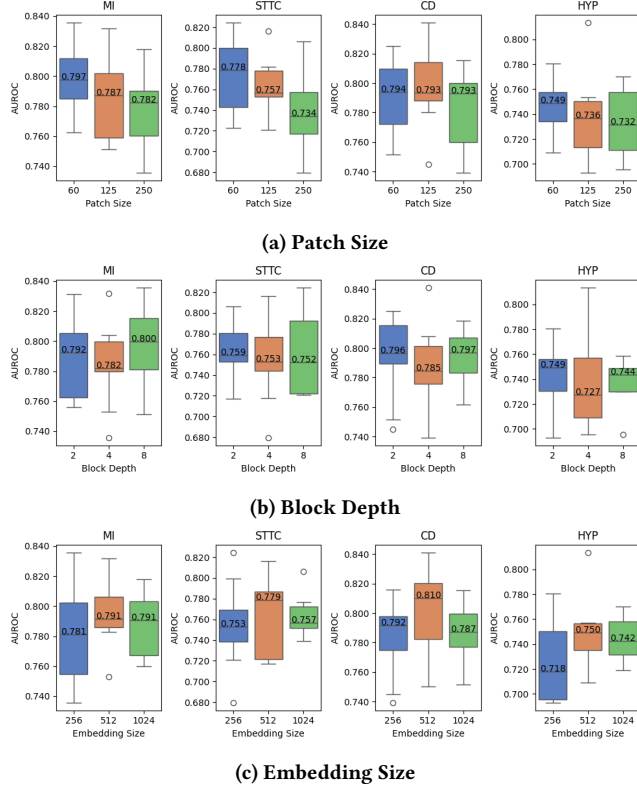


**Figure 3: Impact of the architectural design of the HL-based foundation models.**

Figure 3 shows the linear probing performance for the HL foundation model on downstream tasks depending on architectural design. Due to space limitations, the results for other foundation models are shown in Figure 4 in Appendix C. In this figure, x-axes correspond to the architectural variations (i.e., patch size, the block depth, and the embedding size), y-axes correspond to the performance (i.e., AUROC), and the whiskers of each box plot correspond to the minimum and maximum of AUROC in each row. To compare the different architectural variations of each foundation model, we chose the median AUROC as the primary performance metric and the range between the minimum and maximum AUROC as the secondary stability metric.

We observed that a patch size of 60 consistently yields the highest median AUROC across most tasks. This is particularly evident in the AUROC of MI and CD, where the performance is higher and more consistent, as indicated by the smaller gap between the lowest and highest performance with no outliers. A block depth of 2 provides the best balance between performance and stability. It provides the highest median AUROC across tasks with a smaller difference in min-max AUROC, suggesting a more dependable and stable model design. An embedding size of 512 demonstrates the most effectiveness, displaying the highest median AUROC in multiple tasks and contributing to the stability of the model with a smaller variation in performance metrics.

We applied the same criteria to determine the best settings for the CL and GL foundation models. The optimal setup for the CL foundation model involves using a patch size of 250, a block depth of 2, and an embedding size of 1024, resulting in the highest median AUROC values and stability. The larger patch and embedding positively impact the model’s performance and reliability. Similarly, the optimal setup for the GL foundation model consists of a patch size of 60, a block depth of 2, and an embedding size of 512, closely resembling that of the HL foundation model. This setup yields the highest median AUROC values for most tasks with minimal performance variation, illustrating its stability and reliability.

These findings offer valuable insights into how architectural designs influence the performance of foundation models across various tasks. In the following sections, we will compare the linear probing and fine-tuning performance of these foundation models based on their respective architectural designs chosen in this section.

#### 4.2 Performance of SSL Foundation Models

**Linear Probing Performance.** Table 1 contains a detailed comparison of the linear probing performance of foundation models trained using CL, GL, and HL against a baseline model randomly initialized weights of the encoder. All SSL foundation models outperform the baseline model on all downstream tasks, demonstrating their ability to capture the generalized representations of ECGs.

Among these models, the HL foundation model has the best performance, achieving the highest criteria score (5.2047) and surpassing the CL and GL foundation models. In particular, the HL foundation model achieves the highest AUROC for MI (0.8053) and CD (0.8251), and the GL foundation model showed the highest AUROC for STTC (0.8375), while the CL foundation model excels others in the HYP task (0.8138).

Overall, this evaluation underscores the robustness of the HL foundation model in achieving superior performance across various tasks, suggesting it is a promising method for the ECG foundation model.

**Ablations.** We identified the primary sources of error and understand the trade-offs between different SSL methods through risk decomposition [12] on the SSL linear probing models. Each method was evaluated across four errors: approximation, representation usability, probe generalization, and encoder generalization. Table 2 presents the results across SSL methods over downstream tasks (MI, STTC, CD, and HYP).

- **Approximation Error** indicates the ability of a model to capture the essence of the task. Higher errors suggest that the architecture of the model might be insufficient to represent the complexity of the task. In terms of an average error on all tasks, The GL linear probing model records the lowest errors, indicating that the architecture of the model is better suited for capturing the high-fidelity representation of ECGs.
- **Representation Usability Error** evaluates the usefulness of the model’s learned representations for downstream tasks. Lower errors indicate that the representations of the model are more effectively utilized. The GL linear probing model has the lowest average error on all tasks, demonstrating superior performance

**Table 1: The performance of the linear probed models on SSL foundation models with optimized architectural design, the Random Initialization (weight of the encoder is randomly initialized) models are served as baseline**

Model	Patch Size	Block Depth	Embedding Size	AUROC				AUPRC				Criteria
				MI	STTC	CD	HYP	MI	STTC	CD	HYP	
Random Initialization (Baseline)	250	2	1024	0.6469	0.7872	0.7261	0.7979	0.4120	0.5844	0.5444	0.3724	4.8713
	60	2	512	0.6451	0.7888	0.7242	0.7943	0.4114	0.5821	0.5424	0.3697	4.8580
Contrastive Learning Generative Learning Hybrid Learning	250	2	1024	0.7238	0.8045	0.7382	<b>0.8138</b>	0.4571	0.5481	0.4335	<b>0.3632</b>	4.8867
	60	2	512	0.6453	<b>0.8375</b>	0.7222	0.7655	0.4394	<b>0.6571</b>	0.4802	0.3689	4.9161
	60	2	512	<b>0.8053</b>	0.7805	<b>0.8251</b>	0.7561	<b>0.5942</b>	0.5281	<b>0.6074</b>	0.3080	<b>5.2047</b>

**Table 2: Results of risk decomposition of the fine-tuned downstream models**

		Approx.	Represent. Usability.	Probe. Generaliz.	Encoder. Generaliz.	Total Risk. (Total Error)
CL	MI	0.0930	0.1389	0.0080	0.0380	0.2779
	STTC	0.1159	0.0970	0.0870	-0.0920	0.2080
	CD	0.1110	0.0999	-0.0309	0.0503	0.2303
	HYP	0.1500	0.0669	0.0030	0.0106	0.2306
	AVR.	0.1175	<b>0.1007</b>	0.0168	0.0017	0.2367
GL	MI	0.1000	0.2289	0.0310	-0.0010	0.3589
	STTC	0.1010	0.2009	-0.0019	-0.0190	0.2809
	CD	0.1070	0.2560	0.0169	-0.0517	0.3282
	HYP	0.1459	0.1579	0.0160	-0.0539	0.2660
	AVR.	<b>0.1135</b>	0.2109	<b>0.0155</b>	<b>-0.0314</b>	0.3085
HL	MI	0.0960	0.1509	0.0530	-0.0430	0.2569
	STTC	0.1150	0.0909	-0.0059	0.0209	0.2210
	CD	0.1000	0.0819	0.0180	-0.0124	0.1875
	HYP	0.1480	0.1060	0.0659	-0.0696	0.2503
	AVR.	0.1148	0.1074	0.0328	-0.0260	<b>0.2289</b>

in generating linearly separable and usable representations for downstream tasks.

- **Probe Generalization Error** reflects the ability of the model to generalize learned representations to new data. Lower errors indicate better generalization. In average error, the GL linear probing model presents the lowest error, highlighting the strengths in generalization, potentially making it suitable for applications where robustness to new data is paramount.
- **Encoder Generalization Error** indicates how well the encoder of the model generalizes across different data distributions. Lower errors suggest that the model performs well on diverse datasets. The GL linear probing model proves superior in this regard on average of all tasks, suggesting that GL better captures the underlying high-fidelity representation of ECGs.

**Total Risk.** The aggregate of four errors indicates the balance of model capabilities covering architectural capacity, representation utility, and generalizability. Despite not demonstrating the lowest error in any specific error type, the HL linear probing model displays the lowest average total error across all tasks, showcasing its stability. This stability, in turn, translates into heightened applicability of HL across diverse clinical scenarios. On the contrary, CL and GL linear probing models exhibit constraints, excelling in either representation usability or generalizability. These discoveries yield critical insights into the strengths and limitations of each SSL method, guiding the selection of models tailored to precise clinical requisites.

### 4.3 Real-World Applicability

**Fine-tuning Performance.** Table 3 displays the performance of baseline SL models (our ViT variation and a ResNet) and SSL fine-tuned models.

Among the SL models, the performance of our ViT variation model (6.9715 criteria score) is slightly better than the ResNet model (6.9325 criteria score), indicating the effectiveness of our model’s structure in enhancing the representation of ECGs. The superior performance of the SSL fine-tuned models compared to the SL models suggests that the foundation models leverage extensive unlabeled data during pre-training, enabling them to learn more robust and generalized representations.

The HL fine-tuned model achieves the highest AUROC across all tasks. Additionally, the AUPRC of the HL fine-tuned model exhibited patterns similar to those of the AUROC results. These results indicate that the HL foundation model excelled in recognizing variations in heart signals through the broad range of features from the ECGs due to its balanced pre-training.

**Low Incidence Rates.** Table 4 shows the performance of SSL fine-tuned models and SL model evaluated with varying percentages of case ratios (5%, 2%, 1%). The case ratios are aligned with the real-world incidence rate [17]. See Appendix A.3 for details of refining case ratio. The results represent that AUROC and AUPRC generally decrease as the incidence rate (case ratio) decreases across all learning methods, indicating a drop in model performance with fewer cases.

First, the CL, GL, and HL fine-tuned models consistently outperform the end-to-end SL model across all tasks and case ratios. The SL model has 6.7960 ( a drop of 2.52%) criteria score at 5% of the case ratio, 6.6388 (a drop of 4.77%) at 2%, and 6.407 (a drop of 8.1%) at 1%, respectively.

Meanwhile, the CL fine-tuned model showed 6.8731 ( a drop of 1.64%) criteria score at 5% of the case ratio, 6.7627 (a drop of 3.22%) at 2%, and 6.5826 (a drop of 5.8%) at 1%, respectively. The GL fine-tuned model showed 6.8859 ( a drop of 1.09%) criteria score at 5% of the case ratio, 6.5815 (a drop of 5.46%) at 2%, and 6.4182 (a drop of 7.8%) at 1%, respectively. The HL fine-tuned model showed 6.9496 ( a drop of 1.55%) criteria score at 5% of the case ratio, 6.7643 (a drop of 4.17%) at 2%, and 6.6309 (a drop of 6.06%) at 1%, respectively.

Notably, the HL fine-tuned model shows the best performance with all case ratios compared to other methods. In addition, it tends to maintain performance comparably even though the case ratio is dropped. This trend indicates that the HL fine-tuned model is more robust than the CL and GL fine-tuned models when case ratios are reduced.

**Table 3: The performance of SSL fine-tuned models with optimized architectural design, the end-to-end supervised models served as the baseline**

Model	Patch Size	Block Depth	Embedding Size	AUROC				AUPRC				Criteria
				MI	STTC	CD	HYP	MI	STTC	CD	HYP	
Supervised Learning (ResNet)		1D-ResNet50		0.9370	0.9251	0.9348	0.9146	0.8599	0.8050	0.8726	0.6835	6.9325
Supervised Learning (Our ViT variation)	250	2	1024	0.9369	0.9380	0.9384	0.9071	0.8571	0.8351	0.8810	0.6769	6.9715
	60	2	512	0.9399	0.9309	0.9397	0.9065	0.8652	0.8101	0.8758	0.6820	6.9501
Contrastive Learning	250	2	1024	0.9366	0.9396	0.9318	0.9232	0.8625	0.8318	0.8661	0.6960	6.9876
	60	2	512	0.9384	0.9318	0.9352	0.9168	0.8619	0.8126	0.8686	0.6962	6.9615
Generative Learning Hybrid Learning	60	2	512	<b>0.9446</b>	<b>0.9400</b>	<b>0.9400</b>	<b>0.9291</b>	<b>0.8814</b>	<b>0.8435</b>	<b>0.8778</b>	<b>0.7023</b>	<b>7.0587</b>

**Table 4: Performance of SSL fine-tuned models according to varying case ratios, excluding original case ratios detailed in Table 3**

Model	Case Ratio (%)	AUROC				AUPRC				Criteria
		MI	STTC	CD	HYP	MI	STTC	CD	HYP	
Supervised Learning (Baseline)	5%	0.9185	0.9173	0.9168	0.9039	0.8356	0.8001	0.8371	0.6667	6.7960
	2%	0.9045	0.8968	0.8934	0.9115	0.7974	0.7538	0.8017	0.6797	6.6388
	1%	0.8797	0.8969	0.8576	0.8928	0.7684	0.7462	0.7373	0.6281	6.407
Contrastive Learning	5%	0.9234	0.9191	0.9259	0.9208	0.8475	0.7917	0.8441	0.7006	6.8731
	2%	<b>0.9176</b>	<b>0.9167</b>	0.9104	<b>0.9142</b>	0.8237	<b>0.7866</b>	<b>0.8188</b>	0.6747	6.7627
	1%	0.8991	0.9030	0.8921	<b>0.8995</b>	0.7975	0.7442	0.7995	0.6477	6.5826
Generative Learning	5%	0.9231	<b>0.9312</b>	0.9247	0.9144	0.8408	<b>0.8132</b>	0.8474	0.6911	6.8859
	2%	0.8912	0.8850	0.9067	0.9052	0.7903	0.7103	0.8169	0.6759	6.5815
	1%	0.8756	0.8856	0.8729	0.8850	0.7536	0.7400	0.7666	0.6389	6.4182
Hybrid Learning	5%	<b>0.9294</b>	0.9278	<b>0.9304</b>	<b>0.9246</b>	<b>0.8636</b>	0.8094	<b>0.8564</b>	<b>0.7080</b>	<b>6.9496</b>
	2%	0.9116	0.9142	<b>0.9113</b>	0.9140	<b>0.8349</b>	0.7759	0.8181	<b>0.6843</b>	<b>6.7643</b>
	1%	<b>0.9069</b>	<b>0.9124</b>	<b>0.9053</b>	0.8816	<b>0.8133</b>	<b>0.7773</b>	<b>0.8175</b>	<b>0.6166</b>	<b>6.6309</b>

**Table 5: Performance of SSL fine-tuned models based on varying percentages of labeled data usage, excluding 100% data usage detailed in Table 3**

Model	Data Usage (%)	AUROC				AUPRC				Criteria
		MI	STTC	CD	HYP	MI	STTC	CD	HYP	
Supervised Learning (Baseline)	50%	0.9311	0.9292	0.9313	0.9049	0.8454	0.8112	0.8623	0.6618	6.8772
	25%	0.9170	0.8991	0.9089	0.8935	0.8184	0.7391	0.8111	0.6446	6.6317
	10%	0.9006	0.9047	0.9017	0.8609	0.7717	0.7545	0.8077	0.6028	6.5046
Contrastive Learning	50%	0.9361	0.9325	0.9239	<b>0.9212</b>	0.8561	0.8095	0.8583	0.6910	6.9286
	25%	0.9161	0.9249	0.9140	0.9145	0.8235	0.7859	0.8219	0.6817	6.7825
	10%	0.9022	<b>0.9237</b>	0.9064	<b>0.9010</b>	0.8015	0.7828	0.8029	0.6237	<b>6.6442</b>
Generative Learning	50%	0.9318	0.9238	0.9318	0.9055	0.8586	0.8115	0.8569	0.6689	6.8888
	25%	0.9067	0.9244	0.9236	0.8999	0.8091	0.7906	0.8419	0.6509	6.7471
	10%	0.8885	0.9204	0.8864	0.8883	0.7676	<b>0.7834</b>	0.7774	<b>0.6367</b>	6.5487
Hybrid Learning	50%	<b>0.9420</b>	<b>0.9332</b>	<b>0.9350</b>	0.9178	<b>0.8760</b>	<b>0.8174</b>	<b>0.8609</b>	<b>0.6968</b>	<b>6.9791</b>
	25%	<b>0.9267</b>	<b>0.9259</b>	<b>0.9268</b>	<b>0.9158</b>	<b>0.8467</b>	<b>0.7882</b>	<b>0.8447</b>	<b>0.7084</b>	<b>6.8832</b>
	10%	<b>0.9182</b>	0.9166	<b>0.9112</b>	0.8655	<b>0.8304</b>	0.7613	<b>0.8064</b>	0.5841	6.5937

**Restricted Data Availability.** Table 5 displays the performance of SSL fine-tuned models and SL models evaluated with varying percentages of labeled data usage: 50% (9,806 samples), 25% (4,903 samples), and 10% (1,961 samples). While keeping the original case ratio, the number of labels in our labeled dataset was insufficient to comply with conventional experimental settings such as the SimCLR protocol, which requires data usage percentages of 100%, 10%, and 1%. As a result, we determined the data usage percentage based on the available number of labels.

The results present that as the proportion of labeled data diminished, the performance metrics for all methods declined. This decline is most pronounced at 10% data usage, with notably lower AUROC and AUPRC. The SL model exhibits the sharpest decrease, suggesting its reliance on larger labeled datasets. At 50% data usage,

the SL model demonstrates a criteria score of 6.8772 (a drop of 1.35%). However, its performance declined as data usage dropped to 25% and 10%, with criteria scores of 6.6317 (a drop of 4.87%) and 6.5046 (a drop of 6.7%), respectively.

In contrast, the SSL foundation models show greater robustness to reduced labeled data. The CL fine-tuned model maintains performance across all data usage levels, achieving a criteria score of 6.9286 (a drop of 0.84%) at 50% data usage, 6.7825 (a drop of 2.94%) at 25%, and 6.6442 (a drop of 4.91%) at 10%. Meanwhile, the GL fine-tuned model performs similarly to the SL model at 50% (6.8888, a drop of 1.04%) but shows a slight advantage at lower data usage levels, with criteria scores of 6.7471 (a drop of 3.08%) at 25% and 6.5487 (a drop of 5.93%) at 10%.



The HL fine-tuned model consistently outperforms the others across all tasks, displaying the highest criteria scores at 50% and 25% data usage, achieving 6.9791 (a drop of 1.13%) and 6.8832 (a drop of 2.49%), respectively. However, at 10% data usage, the HL fine-tuned model exhibits larger drops in criteria scores (6.5937, a drop of 6.59%) compared to that of the CL and GL fine-tuned models. Notably, the STTC and HYP tasks demonstrate larger drops in AUROC and AUPRC, compared to the CL and GL fine-tuned models, because of the superior generalizability of CL and GL foundation models on STTC and HYP tasks in Table 1.

In summary, among the foundation models, the HL fine-tuned model demonstrates superior performance when using more than 25% of the data. Interestingly, the CL fine-tuned model shows the smallest performance gap across varying data usage levels, indicating greater stability between cases using 50% and 10% of the data. This result suggests that while the HL fine-tuned model excels with sufficient data, the CL fine-tuned model is more resilient to reductions in data availability.

## 5 Discussion

### 5.1 Answering Research Questions

This section discusses the experimental results and answers the research questions.

**RQ1. Architectural Design.** The selection of architectural design, such as patch size, block depth, and embedding size, plays a crucial role in the performance of foundation models for ECGs.

From Figure 1, we found that the patch size determines the granularity of the input data processed by the model. For the HL and GL methods, a patch size of 60 is optimal, while the CL method performed better with a patch size of 250. Block depth refers to the number of layers or blocks in the model. A block depth of 2 is consistently the most effective across all SSL methods. Embedding size affects the dimensionality of the representations learned by the model. For HL and GL, an embedding size of 512 yields the best performance. However, CL requires an embedding size of 1024 to achieve optimal results.

**RQ2. SSL Methods Comparison.** Different SSL methods have unique strengths and are suited to various ECG analysis tasks.

The GL focuses on reconstructing input data to understand the underlying structure of ECGs. It shows promising results in high-fidelity representation capability, such as STTC tasks. Conversely, CL distinguishes between instances by contrasting similar and dissimilar ECGs, such as HYP tasks.

The HL combines the strengths of both GL and CL. It consistently demonstrates superior capability in encoding complex representations of ECGs, making it effective across various tasks. Combining generative and contrastive objectives allows HL to learn both high-fidelity and discriminative representations of ECGs, leading to high performance in almost downstream tasks in linear probing.

**RQ3. Practical Applicability.** The HL fine-tuned model consistently shows superior performance across all downstream tasks, demonstrating its robustness by learning generalized representations from ECGs due to its balanced pre-training. HL’s robust performance in handling low incidence rates and limited data availability makes it particularly suitable for clinical settings where

labeled data is often scarce [17]. This adaptability ensures that HL can maintain high performance even with reduced datasets, enhancing its practicality for real-world use. However, in a few situations having extremely limited data availability (under 10% of data usage in our experimental settings), the adaptability of CL to data-scarce environments makes it valuable.

### 5.2 Guidance of Foundation Model for ECGs

To develop effective foundation models for ECGs, it is necessary to carefully consider various architectural and methodological aspects. Our findings highlight several key factors that contribute to the optimal performance of these models.

**SSL Method Selection** The effectiveness of the foundation model for cardiac diagnostics is presented in Table 3. Among the results, the HL foundation model is the most robust since the HL approach effectively represents ECGs by balancing both the strengths of GL and CL. In Table 2, the result of risk decomposition also indicates that the HL foundation model well-learned generalized representations of new ECGs when used in downstream tasks and effectively captures the high-fidelity representation of ECGs to generalize across different data distributions, making it highly reliable for practical applications. Once Again, the HL foundation model shows robustness and reliability in clinical settings with varying data from Table 4 and 5. However, the CL foundation model is considerable since it shows the most robust performance under extremely limited data availability (under 10% in our experiment).

**Architectural Design** The ideal structure for the foundation model based on the HL approach is shown in Figure 3. Based on this result, we conjecture that a smaller patch is more effective in detecting subtle patterns and abnormalities by utilizing both local and global contexts of ECGs. A less complex block depth better balances complexity and computational efficiency, while an appropriate embedding size provides adequate representations of the ECGs. However, it’s important to note that this optimal architecture is specific to our task and may differ for other tasks.

By adhering to these guidelines, researchers and practitioners can develop a foundation model well-suited for the complexities and demands of ECG analysis in clinical practice. This approach ensures that the model is robust and practical for real-world medical applications, ultimately advancing the field of cardiac diagnostics and improving patient outcomes.

### 5.3 Limitations and Future Works

**Dynamic Weight Adjustment in Hybrid Loss.** In the HL foundation model, the hybrid loss only combines contrastive and generative loss in a fixed 1:1 ratio, which may not be optimal across different datasets or tasks. Weighting each loss could better capture their contributions. By optimizing these weights, we could enhance model performance and extend its applicability to a broader range of clinical scenarios.

**Generalization to Other ECG Tasks.** We only focused on four ECG classification tasks (MI, STTC, CD, HYP). Broadening the focus to encompass other subsequent tasks (abnormal detection, segmentation, and prediction) as well as clinically significant tasks (arrhythmia detection and analysis of heart rate variability) could offer a more thorough evaluation of the model’s effectiveness.



**Interpretability.** While the presented models demonstrate performance improvement, their interpretability remains a challenge. Developing methods to enhance their interpretability is crucial for gaining clinician trust and facilitating integration into clinical workflows. Future research should explore techniques such as explainable AI (XAI) methods to address this issue.

## 6 Conclusion

Our research focused on developing foundation models for ECGs using SSL methods. We introduced a Hybrid Learning (HL) approach that integrates CL and GL methods to establish a robust foundational model for ECGs in the context of cardiac diagnosis. We investigated various architectural designs of the foundational model and SSL methods to enhance the representation of ECGs. Our study underscores the significant impact of the SSL method and architectural design choice on the robustness of the foundational model. The HL method exhibited exceptional performance in linear probing and fine-tuning for real-world scenarios, highlighting the robustness and practical applicability of the foundation models in real-world applications. This advancement sets the stage for further progress in medical fields, leveraging deep learning methods.

## References

- [1] Salar Abbaspourazad, Oussama Elachqar, Andrew Miller, Saba Emrani, Udhyakumar Nallasamy, and Ian Shapiro. 2024. Large-scale Training of Foundation Models for Wearable Biosignals. In *Proceedings of the Twelfth International Conference on Learning Representations*.
- [2] Josh Achiam, Steven Adler, Sandhini Agarwal, Lama Ahmad, Ilge Akkaya, Florencia Leoni Aleman, Diogo Almeida, Janko Altschmidt, Sam Altman, Shyamal Anadkat, et al. 2023. GPT-4 Technical Report. *arXiv preprint arXiv:2303.08774* (2023).
- [3] Adrian Atienza, Jakob Bardram, and Sadasivan Puthusserypady. 2023. Subject-based Non-contrastive Self-Supervised Learning for ECG Signal Processing. *arXiv preprint arXiv:2305.10347* (2023).
- [4] Alexei Baevski, Wei-Ning Hsu, Qiantong Xu, Arun Babu, Jiatao Gu, and Michael Auli. 2022. Data2vec: A General Framework for Self-Supervised Learning in Speech, Vision and Language. In *Proceedings of the International Conference on Machine Learning*.
- [5] Alexei Baevski, Yuhao Zhou, Abdelrahman Mohamed, and Michael Auli. 2020. Wav2Vec 2.0: A Framework for Self-Supervised Learning of Speech Representations. *Advances in Neural Information Processing Systems* (2020).
- [6] Mathilde Caron, Ishan Misra, Julien Mairal, Priya Goyal, Piotr Bojanowski, and Armand Joulin. 2020. Unsupervised Learning of Visual Features by Contrasting Cluster Assignments. *Advances in Neural Information Processing Systems* (2020).
- [7] Ting Chen, Simon Kornblith, Mohammad Norouzi, and Geoffrey Hinton. 2020. A Simple Framework for Contrastive Learning of Visual Representations. In *Proceedings of the International Conference on Machine Learning*.
- [8] Mingyue Cheng, Qi Liu, Zhiding Liu, Hao Zhang, Rujiao Zhang, and Enhong Chen. 2023. TimeMAE: Self-Supervised Representations of Time Series with Decoupled Masked Autoencoders. *arXiv preprint arXiv:2303.00320* (2023).
- [9] Hsiang-Yun Sherry Chien, Hanlin Goh, Christopher M Sandino, and Joseph Y Cheng. 2022. Maeeg: Masked Auto-encoder for EEG Representation Learning. *arXiv preprint arXiv:2211.02625* (2022).
- [10] Jacob Devlin, Ming-Wei Chang, Kenton Lee, and Kristina Toutanova. 2018. Bert: Pre-training of Deep Bidirectional Transformers for Language Understanding. *arXiv preprint arXiv:1810.04805* (2018).
- [11] Alexey Dosovitskiy, Lucas Beyer, Alexander Kolesnikov, Dirk Weissenborn, Xi-aohua Zhai, Thomas Unterthiner, Mostafa Dehghani, Matthias Minderer, Georg Heigold, Sylvain Gelly, et al. 2020. An Image is Worth 16x16 Words: Transformers for Image Recognition at scale. *arXiv preprint arXiv:2010.11929* (2020).
- [12] Yann Dubois, Tatsunori Hashimoto, and Percy Liang. 2023. Evaluating Self-Supervised Learning via Risk Decomposition. *arXiv preprint arXiv:2302.03068* (2023).
- [13] Jean-Yves Franceschi, Aymeric Dieuleveut, and Martin Jaggi. 2019. Unsupervised Scalable Representation Learning for Multivariate Time Series. *Advances in Neural Information Processing Systems* (2019).
- [14] Daniel Gedon, Antônio H. Ribeiro, Niklas Wahlström, and Thomas Bo Schön. 2021. First Steps Towards Self-Supervised Pretraining of the 12-Lead ECG. *Computing in Cardiology* (2021).
- [15] Kaiming He, Xinlei Chen, Saining Xie, Yanghao Li, Piotr Dollár, and Ross Girshick. 2022. Masked Autoencoders are Scalable Vision Learners. In *Proceedings of the IEEE/CVF Conference on Computer Vision and Pattern Recognition*.
- [16] Kaiming He, Haoqi Fan, Yuxin Wu, Saining Xie, and Ross Girshick. 2020. Momentum Contrast for Unsupervised Visual Representation Learning. In *Proceedings of the IEEE/CVF Conference on Computer Vision and Pattern Recognition*.
- [17] William Hinton, Andrew McGovern, Rachel Coyle, Thang S Han, Pankaj Sharma, Ana Correa, Filipa Ferreira, and Simon de Lusignan. 2018. Incidence and prevalence of cardiovascular disease in English primary care: a cross-sectional and follow-up study of the Royal College of General Practitioners (RCGP) Research and Surveillance Centre (RSC). *British Medical Journal Open* (2018).
- [18] Zhicheng Huang, Xiaojie Jin, Chengze Lu, Qibin Hou, Ming-Ming Cheng, Dongmei Fu, Xiaohui Shen, and Jiashi Feng. 2023. Contrastive Masked Autoencoders are Stronger Vision Learners. *IEEE Transactions on Pattern Analysis and Machine Intelligence* (2023).
- [19] Junguang Jiang, Yang Shu, Jianmin Wang, and Mingsheng Long. 2022. Transferability in Deep Learning: A Survey. *arXiv preprint arXiv:2201.05867* (2022).
- [20] Alistair EW Johnson, Tom J Pollard, Lu Shen, Li-wei H Lehman, Mengling Feng, Mohammad Ghassemi, Benjamin Moody, Peter Szolovits, Leo Anthony Celi, and Roger G Mark. 2016. MIMIC-III, A Freely Accessible Critical Care Database. *Scientific Data* (2016).
- [21] Jiewei Lai, Huixin Tan, Jinliang Wang, Lei Ji, Jun Guo, Baoshi Han, Yajun Shi, Qianjin Feng, and Wei Yang. 2023. Practical Intelligent Diagnostic Algorithm for Wearable 12-lead ECG via Self-Supervised Learning on Large-scale Dataset. *Nature Communications* (2023).
- [22] Han Liu, Zhenjie Zhao, and Q. She. 2021. Self-Supervised ECG Pre-training. *Biomedical Signal Processing and Control* (2021).
- [23] Ziyu Liu, Azadeh Alavi, Minyi Li, and Xiang Zhang. 2024. Self-Supervised Learning for Time Series: Contrastive or Generative? *arXiv preprint arXiv:2403.09809* (2024).
- [24] Temesgen Mehari and Nils Strodthoff. 2022. Self-Supervised Representation Learning from 12-lead ECG Data. *Computers in Biology and Medicine* (2022).
- [25] Yeongyeon Na, Minje Park, Yunwon Tae, and Sunghoon Joo. 2024. Guiding Masked Representation Learning to Capture Spatio-Temporal Relationship of Electrocardiogram. *arXiv preprint arXiv:2402.09450* (2024).
- [26] Yuqi Nie, Nam H Nguyen, Phanwadee Sinthong, and Jayant Kalagnanam. 2022. A Time Series is Worth 64 Words: Long-term Forecasting with Transformers. *arXiv preprint arXiv:2211.14730* (2022).
- [27] Manuel T Nonnenmacher, Lukas Oldenburg, Ingo Steinwart, and David Reeb. 2022. Utilizing Expert Features for Contrastive Learning of Time-Series Representations. In *Proceedings of the International Conference on Machine Learning*.
- [28] Quentin Rebjock, Baris Kurt, Tim Januschowski, and Laurent Callot. 2021. Online False Discovery Rate Control for Anomaly Detection in Time Series. *Advances in Neural Information Processing Systems* (2021).
- [29] Antônio H. Ribeiro, Gabriela M.M. Paixao, Emilly M. Lima, Manoel Horta Ribeiro, Marcelo M. Pinto Filho, Paulo R. Gomes, Derick M. Oliveira, Wagner Meira Jr, Thômas B Schon, and Antonio Luiz P. Ribeiro. 2021. CODE-15%: A Large Scale Annotated Dataset of 12-lead ECGs. (2021). <https://doi.org/10.5281/zenodo.4916206>
- [30] Antonio Luiz P. Ribeiro, Antônio H. Ribeiro, Gabriela M.M. Paixao, Emilly M. Lima, Manoel Horta Ribeiro, Marcelo M. Pinto Filho, Paulo R. Gomes, Derick M. Oliveira, Wagner Meira Jr, Thômas B Schon, and Ester C Sabino. 2021. SaMI-Trop: 12-lead ECG Traces with Age and Mortality Annotations. (2021). <https://doi.org/10.5281/zenodo.4905618>
- [31] Pritam Sarkar and A. Etemad. 2020. Self-Supervised ECG Representation Learning for Emotion Recognition. *IEEE Transactions on Affective Computing* (2020).
- [32] Pritam Sarkar and Ali Etemad. 2020. Self-Supervised Learning for ECG-based Emotion Recognition. In *Proceedings of the IEEE International Conference on Acoustics, Speech and Signal Processing*.
- [33] Michal Seják, Jakub Sido, and David Zahour. 2023. IKEM Dataset v1.0.0. (2023). <https://doi.org/10.5281/zenodo.8393007>
- [34] Cathie Sudlow, John Gallacher, Naomi Allen, Valerie Beral, Paul Burton, John Danesh, Paul Downey, Paul Elliott, Jane Green, Martin Landray, et al. 2015. UK Biobank: An Open Access Resource for Identifying the Causes of A Wide Range of Complex Diseases of Middle and Old Age. *PLoS Medicine* (2015).
- [35] Fan-Keng Sun, Chris Lang, and Duane Boning. 2021. Adjusting for Autocorrelated Errors in Neural Networks for Time Series. *Advances in Neural Information Processing Systems* (2021).
- [36] Patrick Wagner, Nils Strodthoff, Ralf-Dieter Boussejot, Dieter Kreiseler, Fatima I Lunze, Wojciech Samek, and Tobias Schaeffter. 2020. PTB-XL, a large publicly available electrocardiography dataset. *Scientific data* (2020).
- [37] Yihe Wang, Yu Han, Haishuai Wang, and Xiang Zhang. 2024. Contrast Everything: A Hierarchical Contrastive Framework for Medical Time-series. *Advances in Neural Information Processing Systems* (2024).
- [38] Sanghyun Woo, Shoubhik Debnath, Ronghang Hu, Xinlei Chen, Zhuang Liu, In So Kweon, and Saining Xie. 2023. ConvNext v2: Co-designing and Scaling Convnets with Masked Autoencoders. In *Proceedings of the IEEE/CVF Conference on Computer Vision and Pattern Recognition*.
- [39] Zhenda Xie, Zheng Zhang, Yue Cao, Yutong Lin, Jianmin Bao, Zhuliang Yao, Qi Dai, and Han Hu. 2022. SIMMIM: A Simple Framework for Masked Image Modeling. In *Proceedings of the IEEE/CVF Conference on Computer Vision and Pattern Recognition*.
- [40] Ling Yang and Shenda Hong. 2022. Unsupervised Time-Series Representation Learning with Iterative Bilinear Temporal-Spectral Fusion. In *Proceedings of the International Conference on Machine Learning*.
- [41] Hugo Yèche, Gideon Dresdner, Francesco Locatello, Matthias Hüser, and Gunnar Rätsch. 2021. Neighborhood Contrastive Learning Applied to Online Patient Monitoring. In *Proceedings of the International Conference on Machine Learning*.
- [42] Zhihan Yue, Yujing Wang, Juanyong Duan, Tianmeng Yang, Congrui Huang, Yunhai Tong, and Bixiong Xu. 2022. TS2VEC: Towards Universal Representation of Time Series. In *Proceedings of the AAAI Conference on Artificial Intelligence*.
- [43] George Zerveas, Srideepika Jayaraman, Dhaval Patel, Anuradha Bhamidipaty, and Carsten Eickhoff. 2021. A Transformer-based Framework for Multivariate Time Series Representation Learning. In *Proceedings of the 27th ACM SIGKDD Conference on Knowledge Discovery and Data Mining*.

## APPENDIX

### A Data sets

#### A.1 Summary

This section describes the various public datasets used in our study, including MIMIC-IV, CODE15, UK Biobank, SaMi-Trop, IKEM, and PTB-XL. From these datasets, we separate the two datasets: unlabeled dataset and labeled dataset. The summaries of each dataset are presented in Table 6 and 7, including demographic information, the number of samples, and specific details about the data collection and characteristics.

**Table 6: Summary of the unlabeled dataset**

		Unlabeled				
		MIMIC	CODE15	BIOBANK	SAMI	IKEM
Demographic Information	Country	USA	USA	UK	Brazil	Czech Republic
	#Patients	161,352	233,770	15,365	1,959	30,290
Statistics	#Sample	800,035	341,292	50,780	1,631	98,130
	#Leads	12	12	12	12	12
	MV-unit	0.005	1	0.005	1	0.004
	Duration(s)	10	10	10	10	10
	Sampling rate(Hz)	500	400	500	400	500

**Table 7: Summary of the labeled dataset**

		Labeled			
		PTB-XL			
Label		MI	STTC	CD	HYP
Demographic Information	#Patients	5,466	5,107	4,897	2,648
	Case ratio	0.2524	0.2382	0.2211	0.1209
Statistics	#Sample	6,886	5,788	5,772	2,819
	#Leads	12	12	12	12
	Length	5,000	5,000	5,000	5,000
	Duration(s)	10	10	10	10
	Sampling Rate(Hz)	500	500	500	500

**MIMIC-IV** [20]. is an extensive database that contains comprehensive data on patients admitted to a tertiary academic medical center in Boston, MA, USA. The database provides information about each hospitalized patient, including laboratory measurements, medications administered, documented vital signs, and other relevant medical data. The primary aim of this database is to support healthcare research.

**CODE15** [29]. is a dataset of 345,779 ECG exams from 233,770 patients. The ECGs were sampled at a rate of 400 Hz and had varying durations but were standardized to ECGs of 4096 points by filling them with zeros on both sides.

**UK Biobank** [34]. is a publicly available dataset containing data on 500,000 individuals from the United Kingdom. This population-based study includes individuals aged 40 to 69 recruited between 2006 and 2010. Resting 12-lead ECGs and interval measurements were available for 15,365 participants, and 13,314 were included in the analysis after excluding those with AF on ECG or AF identified from self-reports at baseline or electronic healthcare records.

**SaMi-Trop** [30]. is a dataset from a prospective cohort study funded by the NIH. It includes 1,959 patients with chronic Chagas cardiomyopathy. It aims to evaluate the usefulness of a clinical prediction rule based on ECG, brain natriuretic peptide (BNP) levels, and other biomarkers in clinical practice. A subset of the SaMi-Trop dataset with annotations of age and mortality and the correspondent ECG traces is available.

**IKEM** [33]. is a dataset of 12-lead ECG recordings collected from patients examined by the cardiology or diabetology sections at the Institute for Clinical and Experimental Medicine (IKEM) in Prague, Czech Republic. The recordings were sampled at a rate of 500 Hz for 10 seconds each. Each entry in the dataset includes raw ECG recordings paired with an anonymized unique patient ID, which groups ECG recordings belonging to the same patient.

**PTB-XL** [36]. is a large dataset of 21,799 clinical 12-lead ECGs from 18,869 patients of 10-second length. The raw waveform data was annotated by up to two cardiologists, who assigned potentially multiple ECG statements to each record. In total, 71 different ECG statements conform to the SCP-ECG standard and cover diagnostic, form, and rhythm statements.

#### A.2 Characteristics of ECG Annotations

This section elaborates on the annotated classes used in the study, including MI, STTC, CD, and HYP. It includes descriptions of each condition, significance, and typical ECG characteristics.

**Myocardial Infarction (MI).** MI, commonly known as a heart attack, involves the interruption of blood supply to a part of the heart, causing heart cells to die. This is typically caused by a blockage in one or more coronary arteries due to plaque (a mix of fat, cholesterol, and other substances). The ECG of a person suffering from MI may show abnormal Q waves, elevation or depression of the ST segment, and T wave inversions. Diagnosing MI involves identifying these specific patterns on different parts of the ECG.

**ST/T Changes (STTC).** STTC on an ECG can indicate various conditions, including cardiac ischemia, electrolyte imbalances, and other myocardial injuries. The ST segment and T wave are parts of the ECG cycle associated with the heart's electrical recovery (repolarization) following a contraction. ST segment elevations can indicate acute myocardial injury (like in the case of an ongoing heart attack), while ST depressions and T wave inversions can suggest coronary ischemia or other cardiac problems.

**Conduction Disturbance (CD).** CD occurs when the heart's electrical impulses are delayed or blocked at certain points in the heart's conduction system (such as the AV node or the His-Purkinje system). This can lead to arrhythmias or irregular heartbeats. ECG patterns may include prolonged PR intervals, widened QRS complexes, or abnormal QRS morphologies, depending on where the blockage occurs. Conditions such as Bundle Branch Blocks or AV blocks are examples.

**Hypertrophy (HYP).** HYP in the cardiac context usually refers to the thickening of the heart muscle, typically the left ventricle, which can be caused by chronic high blood pressure or other diseases that increase the heart's workload. ECG signs of hypertrophy

involve larger-than-normal voltage in QRS complexes, changes in the ST segment and T wave, and a shift in the axis of the QRS wave. These changes reflect increased muscle mass and altered electrical conduction due to thickening walls.

Each task requires the AI model to recognize specific and often subtle variations in ECG waveforms to classify the type of cardiac event or condition accurately. The performance of these tasks in AI models, as measured by AUROC, indicates how well these patterns can be detected and classified against a backdrop of standard and other abnormal patterns.

### A.3 Low Incidence Rates Settings

To evaluate the performance of models based on the incidence rates of various diseases, we established experimental settings corresponding to 1%, 5%, and 25% incidence rates. Given the varying amounts of data and differing incidence rates in the PTB-XL dataset, it was necessary to create standardized conditions for each disease. Specifically, we randomly sampled 7,000 instances for each disease to align with the target incidence rates. For example, to create a dataset with a 1% incidence rate for MI, we randomly selected 70 MI-labeled samples and 6,930 non-MI samples. This method allowed us to build a total of 12 experimental datasets, each reflecting different incidence rates (1%, 5%, 25%) across four diseases.

## B Evaluation Metrics

### B.1 AUROC and AUPRC Calculations

This section explains the evaluation metrics used in the study, including the calculation of Area Under the Receiver Operating Characteristic (AUROC) and Area Under the Precision-Recall Curve (AUPRC). It also provides the formulas and interpretation guidelines for these metrics.

**AUROC.** The Area Under the Receiver Operating Characteristic (AUROC) curve is a statistical measure that evaluates the performance of binary classification models. AUROC plots the True Positive Rate (TPR) versus the False Positive Rate (FPR) at different threshold settings. It represents the probability of a classifier ranking a randomly chosen positive instance higher than a randomly chosen negative one. An AUC of 1 indicates perfect classification, while an AUC of 0.5 suggests performance equivalent to random guessing. AUROC is useful for evaluating models on imbalanced datasets as it is not influenced by class label distribution.

**AUPRC.** The Area Under the Precision-Recall Curve (AUPRC) provides a measure to evaluate binary classification model performance, especially under class imbalance. Unlike AUROC, which plots TPR against FPR, PRC plots Precision (true positives to all predicted positives) against Recall (equivalent to TPR). A higher AUPRC value represents better performance in distinguishing between classes under imbalanced class distributions.

## C Complete Results

This section provides the entire experimental results. The initial stage involved pre-training 81 distinct foundation models (all combinations of three patch sizes, three block depths, three embedding sizes, and three SSL methods) on a large-scale dataset, including 1.3 million unlabeled ECGs.

### C.1 Linear Probing Results

In linear probing, an entire performance of different SSL foundation model architectures (e.g., patch size, block depth, embedding size) in Table 8 and 9. Figure 3 and 4 show the tendency of performance according to the architectural design. This section should include AUROC and AUPRC for various settings, demonstrating how each parameter affects model performance.

### C.2 Fine-tuning Results

The performance of different foundation model architectures (e.g., patch size, block depth, embedding size) in fine-tuning is summarized in Table 10 and 11. We comprehensively compare AUROC and AUPRC across various architectural designs on each SSL method.

Received 8 August 2024



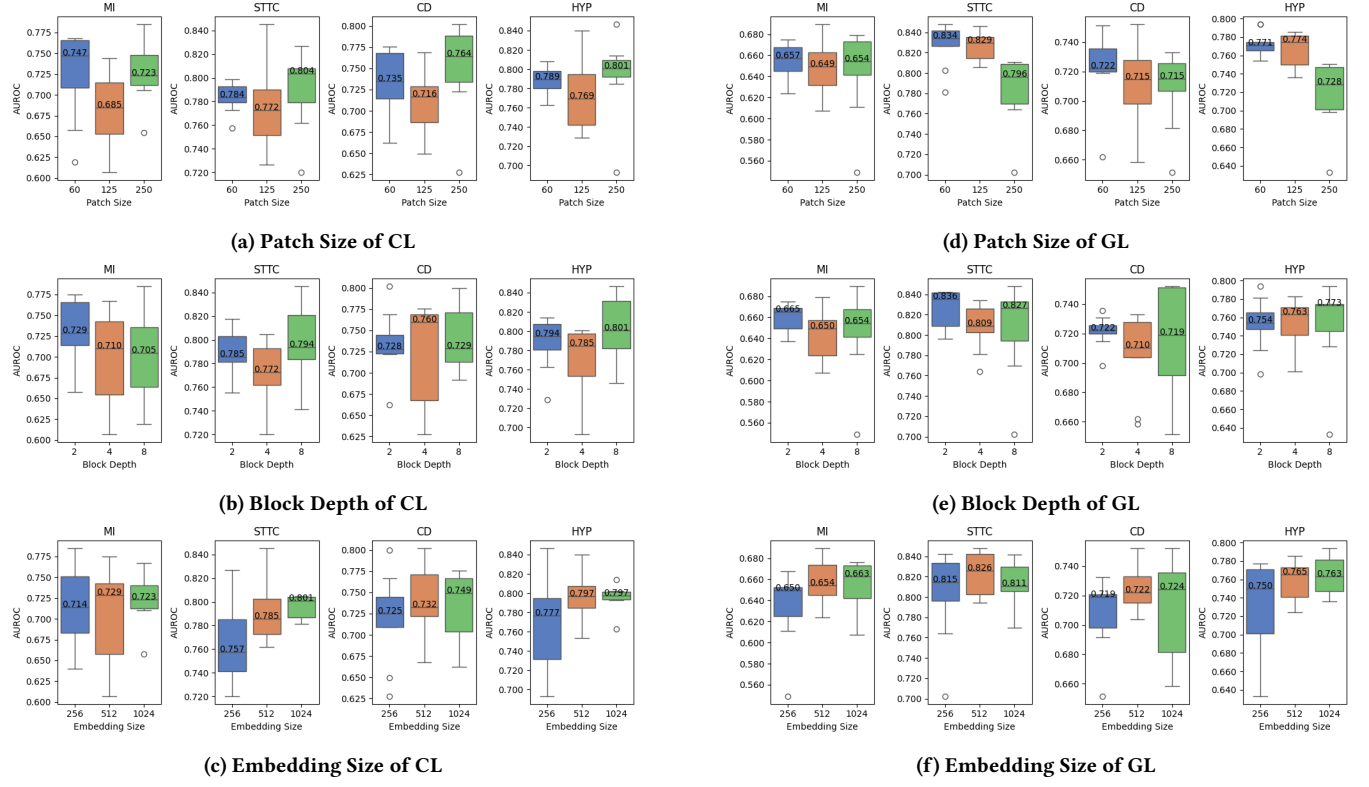


Figure 4: Impact of the architectural design of the CL (left) and GL (right) foundation models.

Table 10: AUROC of the CL, GL, and HL fine-tuned models

Case	Patch Size	Block Depth	Embedding Size	AUROC												Criteria		
				MI			STTC			CD			HYP					
				CL	GL	HL	CL	GL	HL	CL	GL	HL	CL	GL	HL	CL	GL	HL
0	60	2	256	0.9346	0.9408	0.9418	0.9381	0.9335	0.9413	0.9349	0.9352	0.9364	0.9273	0.9198	0.9257	6.9978	6.9671	7.0304
1	60	2	512	0.9406	0.9384	0.9446	0.9386	0.9318	0.9400	0.9389	0.9352	0.9400	0.9229	0.9168	0.9291	6.9932	6.9615	7.0587
2	60	2	1024	0.9324	0.9353	0.9444	0.9356	0.9333	0.9398	0.9320	0.9368	0.9360	0.9193	0.9143	0.9237	6.9464	6.9425	7.0287
3	60	4	256	0.9383	0.9411	0.9444	0.9366	0.9351	0.9364	0.9382	0.9329	0.9378	0.9285	0.9128	0.9274	7.0038	6.9467	7.0200
4	60	4	512	0.9333	0.9300	0.9472	0.9395	0.9377	0.9376	0.9349	0.9367	0.9399	0.9229	0.9180	0.9254	6.9640	6.9412	7.0425
5	60	4	1024	0.9355	0.9365	0.9427	0.9347	0.9370	0.9398	0.9398	0.9360	0.9365	0.9237	0.9066	0.9257	6.9613	6.9485	7.0321
6	60	8	256	0.9303	0.9379	0.9434	0.9393	0.9349	0.9434	0.9367	0.9396	0.9428	0.9210	0.9196	0.9291	6.9742	6.9909	7.0605
7	60	8	512	0.9330	0.9390	0.9453	0.9390	0.9353	0.9368	0.9342	0.9333	0.9366	0.9230	0.9151	0.9339	6.9887	6.9520	7.0555
8	60	8	1024	OOM	0.9364	OOM	OOM	0.9330	OOM	OOM	0.9364	OOM	OOM	0.9150	OOM	OOM	6.9433	OOM
9	125	2	256	0.9406	0.9387	0.9434	0.9426	0.9385	0.9396	0.9388	0.9337	0.9415	0.9272	0.9167	0.9234	7.0448	6.9698	7.0376
10	125	2	512	0.9345	0.9389	0.9406	0.9383	0.9420	0.9412	0.9379	0.9362	0.9391	0.9225	0.9191	0.9213	6.9884	7.0090	7.0199
11	125	2	1024	0.9397	0.9427	0.9452	0.9360	0.9393	0.9403	0.9338	0.9400	0.9425	0.9198	0.9185	0.9245	6.9785	6.9982	7.0510
12	125	4	256	0.9337	0.9404	0.9432	0.9354	0.9361	0.9370	0.9330	0.9361	0.9408	0.9174	0.9137	0.9252	6.9373	6.9565	7.0357
13	125	4	512	0.9377	0.9396	0.9448	0.9347	0.9360	0.9398	0.9352	0.9363	0.9449	0.9292	0.9195	0.9307	7.0089	6.9980	7.0744
14	125	4	1024	0.9375	0.9387	0.9461	0.9353	0.9370	0.9417	0.9393	0.9369	0.9390	0.9190	0.9157	0.9219	6.9977	6.9777	7.0457
15	125	8	256	0.9407	0.9393	0.9434	0.9384	0.9359	0.9413	0.9367	0.9376	0.9399	0.9254	0.9220	0.9163	7.0105	6.9696	7.0175
16	125	8	512	0.9402	0.9330	0.9433	0.9377	0.9412	0.9378	0.9384	0.9367	0.9446	0.9235	0.9178	0.9207	6.9950	6.9825	7.0156
17	125	8	1024	OOM	0.9410	OOM	OOM	0.9370	OOM	OOM	0.9344	OOM	OOM	0.9095	OOM	OOM	6.9756	OOM
18	250	2	256	0.9393	0.9369	0.9442	0.9429	0.9390	0.9406	0.9335	0.9380	0.9428	0.9276	0.9230	0.9253	7.0220	7.0087	7.0511
19	250	2	512	0.9405	0.9346	0.9418	0.9394	0.9349	0.9390	0.9382	0.9348	0.9410	0.9211	0.9214	0.9240	7.0196	6.9685	7.0281
20	250	2	1024	0.9366	0.9346	0.9435	0.9396	0.9373	0.9366	0.9318	0.9389	0.9381	0.9232	0.9117	0.9202	6.9876	6.9494	7.0128
21	250	4	256	0.9368	0.9379	0.9413	0.9339	0.9346	0.9394	0.9319	0.9368	0.9432	0.9234	0.9183	0.9256	6.9834	6.9701	7.0477
22	250	4	512	0.9409	0.9346	0.9437	0.9337	0.9338	0.9406	0.9438	0.9358	0.9415	0.9230	0.9249	0.9215	7.0296	6.9679	7.0405
23	250	4	1024	0.9349	0.9409	0.9452	0.9369	0.9370	0.9393	0.9333	0.9365	0.9393	0.9249	0.9259	0.9203	6.9885	6.9990	7.0200
24	250	8	256	0.9382	0.9387	OOM	0.9397	0.9326	OOM	0.9372	0.9393	OOM	0.9219	0.9272	OOM	7.0019	6.9946	OOM
25	250	8	512	0.9391	0.9377	OOM	0.9384	0.9359	OOM	0.9361	0.9441	OOM	0.9216	0.9125	OOM	7.0120	6.9835	OOM
26	250	8	1024	OOM	0.9409	OOM	OOM	0.9403	OOM	OOM	0.9350	OOM	OOM	0.9097	OOM	OOM	6.9884	OOM

**Table 11: AUPRC of the CL, GL, and HL fine-tuned models**

Case	Patch Size	Block Depth	Embedding Size	AUPRC												Criteria		
				MI			STTC			CD			HYP			CL	GL	HL
				CL	GL	HL	CL	GL	HL	CL	GL	HL	CL	GL	HL			
0	60	2	256	0.8580	0.8644	0.8732	0.8263	0.8164	0.8366	0.8771	0.8660	0.8736	0.7015	0.6910	0.7018	6.9978	6.9671	7.0304
1	60	2	512	0.8647	0.8619	0.8814	0.8176	0.8126	0.8435	0.8752	0.8686	0.8778	0.6947	0.6962	0.7023	6.9932	6.9615	7.0587
2	60	2	1024	0.8549	0.8542	0.8786	0.8240	0.8134	0.8354	0.8636	0.8657	0.8742	0.6846	0.6895	0.6966	6.9464	6.9425	7.0287
3	60	4	256	0.8610	0.8710	0.8753	0.8215	0.8207	0.8236	0.8786	0.8633	0.8775	0.7011	0.6698	0.6976	7.0038	6.9467	7.0200
4	60	4	512	0.8456	0.8464	0.8810	0.8326	0.8188	0.8337	0.8654	0.8697	0.8826	0.6898	0.6839	0.6951	6.9640	6.9412	7.0425
5	60	4	1024	0.8589	0.8629	0.8746	0.8168	0.8261	0.8365	0.8770	0.8644	0.8788	0.6749	0.6790	0.6975	6.9613	6.9485	7.0321
6	60	8	256	0.8570	0.8601	0.8779	0.8304	0.8246	0.8389	0.8712	0.8743	0.8847	0.6883	0.6999	0.7003	6.9742	6.9909	7.0605
7	60	8	512	0.8586	0.8653	0.8828	0.8319	0.8172	0.8331	0.8709	0.8653	0.8766	0.6981	0.6815	0.7104	6.9887	6.9520	7.0555
8	60	8	1024	OOM	0.8588	OOM	OOM	0.8167	OOM	OOM	0.8675	OOM	OOM	0.6795	OOM	OOM	6.9433	OOM
9	125	2	256	0.8686	0.8626	0.8803	0.8439	0.8317	0.8339	0.8745	0.8678	0.8807	0.7086	0.6801	0.6948	7.0448	6.9698	7.0376
10	125	2	512	0.8527	0.8665	0.8735	0.8258	0.8350	0.8365	0.8813	0.8753	0.8796	0.6954	0.6960	0.6881	6.9884	7.0090	7.0199
11	125	2	1024	0.8668	0.8728	0.8799	0.8209	0.8295	0.8363	0.8729	0.8740	0.8835	0.6886	0.6814	0.6988	6.9785	6.9982	7.0510
12	125	4	256	0.8574	0.8671	0.8747	0.8199	0.8223	0.8315	0.8730	0.8695	0.8806	0.6675	0.6713	0.7027	6.9373	6.9565	7.0357
13	125	4	512	0.8634	0.8649	0.8809	0.8291	0.8261	0.8339	0.8711	0.8714	0.8841	0.7085	0.7042	0.7153	7.0089	6.9980	7.0744
14	125	4	1024	0.8638	0.8683	0.8828	0.8282	0.8222	0.8400	0.8806	0.8737	0.8794	0.6940	0.6852	0.6948	6.9977	6.9777	7.0457
15	125	8	256	0.8702	0.8637	0.8749	0.8255	0.8176	0.8373	0.8764	0.8744	0.8820	0.6972	0.6791	0.6824	7.0105	6.9696	7.0175
16	125	8	512	0.8651	0.8551	0.8782	0.8266	0.8352	0.8271	0.8747	0.8725	0.8867	0.6888	0.6910	0.6772	6.9950	6.9825	7.0156
17	125	8	1024	OOM	0.8714	OOM	OOM	0.8274	OOM	OOM	0.8646	OOM	OOM	0.6903	OOM	OOM	6.9756	OOM
18	250	2	256	0.8699	0.8643	0.8773	0.8410	0.8347	0.8412	0.8694	0.8787	0.8837	0.6984	0.6941	0.6960	7.0220	7.0087	7.0511
19	250	2	512	0.8687	0.8576	0.8737	0.8373	0.8178	0.8289	0.8730	0.8742	0.8835	0.7014	0.6932	0.6962	7.0196	6.9685	7.0281
20	250	2	1024	0.8625	0.8562	0.8788	0.8318	0.8299	0.8277	0.8661	0.8713	0.8715	0.6960	0.6695	0.6964	6.9876	6.9494	7.0128
21	250	4	256	0.8670	0.8696	0.8758	0.8158	0.8217	0.8399	0.8724	0.8733	0.8846	0.7022	0.6779	0.6979	6.9834	6.9701	7.0477
22	250	4	512	0.8679	0.8542	0.8791	0.8354	0.8195	0.8428	0.8825	0.8720	0.8823	0.7024	0.6931	0.6890	7.0296	6.9679	7.0405
23	250	4	1024	0.8568	0.8703	0.8800	0.8302	0.8236	0.8375	0.8693	0.8691	0.8773	0.7022	0.6957	0.6811	6.9885	6.9990	7.0200
24	250	8	256	0.8658	0.8694	OOM	0.8364	0.8182	OOM	0.8698	0.8762	OOM	0.6929	0.6930	OOM	7.0019	6.9946	OOM
25	250	8	512	0.8677	0.8600	OOM	0.8300	0.8279	OOM	0.8772	0.8854	OOM	0.7019	0.6800	OOM	7.0120	6.9835	OOM
26	250	8	1024	OOM	0.8684	OOM	OOM	0.8404	OOM	OOM	0.8699	OOM	OOM	0.6838	OOM	OOM	6.9884	OOM